

Inhomogeneity and nonlinear screening in gapped bilayer graphene

D. S. L. Abergel,¹ E. Rossi,² and S. Das Sarma¹

¹*Condensed Matter Theory Center, Department of Physics,
University of Maryland, College Park, MD 20742, USA.*

²*Department of Physics, College of William and Mary, Williamsburg, VA 23187, USA.*

We demonstrate that for gapped bilayer graphene, the nonlinear nature of the screening of the external disorder potential and the resulting inhomogeneity of the electron liquid are crucial for describing the electronic compressibility. In particular, a direct calculation of the charge landscape via a numerical Thomas-Fermi energy functional method along with the appropriate bulk averaging procedure captures all the essential physics, including the interplay between the band gap and the inhomogeneity. In contrast, traditional diagrammatic methods of many-body theory do not include this inhomogeneity and therefore fail to reproduce experimental data accurately, particularly at low carrier densities.

The electronic compressibility (or, equivalently, $\frac{d\mu}{dn}$ where μ is the chemical potential and n the excess carrier density induced by gating or doping) in bilayer graphene (BLG) [1–3] has become a property of great importance recently due to various experimental works purporting to describe the gapped BLG ground state caused either by external gating [4] or by intrinsic electron-electron interactions [5]. It has been shown experimentally [6] and theoretically [7] in BLG that the inhomogeneity in the charge landscape is strong in samples with a high degree of disorder both with and without a gap. The disorder-induced inhomogeneity is particularly strong at low average carrier densities, and a proper description of the compressibility must include the inhomogeneity nonperturbatively. This has not yet been accomplished theoretically.

In this Letter, we describe two possible approaches to this problem, namely, the standard ensemble-averaged perturbative diagrammatic theory of the electron-impurity interaction from many-body physics, and an inherently non-perturbative density-functional approach. We show that diagrammatic theories fail because they assume a homogeneous density distribution including the disorder effects only perturbatively. Also, when an energy gap is present (which we parameterize by the interlayer potential asymmetry u [8]), the interplay between the gap and the nonlinearity of the screening [7, 9] is crucial at low average carrier density since there are large spatial regions of the system where there is vanishing charge density, even at finite average density. In this situation the system is in a mixed (and highly spatially inhomogeneous) state between incompressible and compressible regions. Although standard many-body theories work well at high carrier density where disorder effects can formally be included perturbatively since the spatial density fluctuations are small, they cannot describe this mixed state. In contrast, a non-perturbative self-consistent Thomas-Fermi theory (TFT) that includes disorder and which should be construed as a poor-man's density functional theory (DFT) is able to take into account nonlinear screening effects and therefore capture

the strong density inhomogeneities induced by disorder. Since the compressibility is a thermodynamic property of the ground state, this self-consistent formalism, in conjunction with an appropriately-chosen averaging procedure, gives results which are in qualitative agreement with experimental measurements even at low average carrier densities where the spatial density fluctuations are large. This situation is qualitatively different in monolayer graphene [3, 10–13] where there is no band gap and hence the screening nonlinearity has a much smaller effect on the compressibility since there is no mixed phase.

We begin by describing the diagrammatic theory for the electron-impurity interaction. The compressibility is given by $\frac{1}{n^2} \frac{dn}{d\mu}$ and therefore calculating $\frac{d\mu}{dn}$ is equivalent to obtaining the inverse compressibility [14]. We show results for the self-consistent Born approximation (SCBA) defined by the self-energy

$$\Sigma_{\alpha}^{\text{SCBA}}(\mathbf{k}, E) = n_i \sum_{\mathbf{k}', \alpha'} \frac{|V_D(\mathbf{k} - \mathbf{k}')|^2 F_{\alpha\alpha'}(\mathbf{k}, \mathbf{k}')}{E - E_{\alpha'\mathbf{k}'} + \Sigma_{\alpha'}(\mathbf{k}', E)} \quad (1)$$

and the Born approximation (BA) where $\Sigma_{\alpha}^{\text{BA}}(\mathbf{k}, E)$ is found by substituting $\Sigma_{\alpha'}(\mathbf{k}', E) \rightarrow i\eta$ in the denominator [14]. In these equations, $V_D(\mathbf{k})$ is the screened impurity potential

$$V_D(\mathbf{k}) = \frac{2\pi e^2}{\kappa(k + q_s)} e^{-kd}, \quad q_s = \frac{2\pi e^2}{\kappa} \rho_0(\mu) \quad (2)$$

with q_s being the screening wave vector in the standard static random phase approximation, $F_{\alpha\alpha'}(\mathbf{k}, \mathbf{k}')$ is the wave function overlap of the initial and final states in the scattering process, $E_{\alpha\mathbf{k}}$ is the energy of an electron with wave vector \mathbf{k} in band α , κ is the dielectric constant of the environment, and η is a positive infinitesimal. Note that the assumption of a homogeneous charge landscape enters both in the Green's function via $E_{\alpha'\mathbf{k}'}$ and in the screening via q_s . Consistent with experimental findings [1], we take the disorder to be arising from random quenched unintentional charged impurities in the BLG environment with a 2D impurity density of n_i separated from the graphene layer by an average distance of

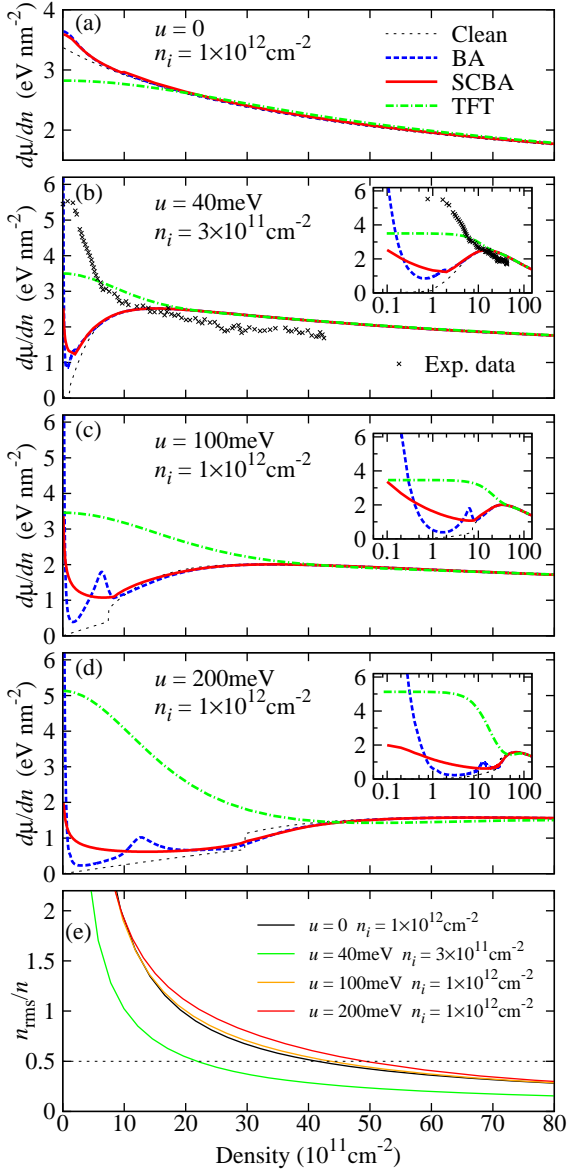


FIG. 1. (Color online) (a)–(d) $\frac{d\mu}{dn}$ for three different values of the band gap and impurity density for all the theories we discuss. The legend in (a) applies to panels (a)–(d), and the insets show the same data as the main plots but for a logarithmic density scale. The experimental data in panel (b) is taken from Fig. 2 of Ref. 4. (e) The density fluctuation due to disorder for panels (b)–(d). The dotted line at $n_{\text{rms}}/n = 0.5$ is included as a guide for the eye.

d. Then, $\frac{d\mu}{dn}$ is found from the inverse density of states (DOS) at the Fermi energy $\frac{d\mu}{dn} = \frac{1}{\rho(\mu)}$.

The calculated $\frac{d\mu}{dn}$ for the clean case [3], the BA, and the SCBA are shown in Figs. 1(a)–(d) as a function of the carrier density. The insets show the same data on a logarithmic scale to emphasize the low-density features. In the ungapped case shown in Fig. 1(a), the BA and SCBA are essentially the same as the clean limit.

When a band gap is present, as in Figs. 1(b)–(d), the

clean limit shows a clear step occurring at the density $\tilde{n} = u^2/(\hbar^2 v_F^2 \pi)$ which marks the density where the chemical potential leaves the sombrero region of the band structure and the topology of the Fermi surface changes from a ring to a disc [2]. For $n \gg \tilde{n}$ the BA and SCBA are similar to the clean limit, but at low to moderate density $n \lesssim \tilde{n}$, the strong modification of the DOS near the band edge [14] implies that $\frac{d\mu}{dn}$ is enhanced relative to the clean system, but is still a decreasing function as n becomes small. There is also a sharp divergence in the BA and SCBA for very small n which is not observed experimentally [4]. Additional structure for $n < \tilde{n}$ in the BA comes from the non-trivial shape of the DOS near $\mu = u$ in that approximation [14]. In Fig. 1(b) we show experimental data for the gapped regime [15]. We see that a broad peak forms in the experimental data at low density in complete qualitative contrast to the BA and SCBA theoretical results. Therefore, these theories totally fail to capture the essential physics of the gapped system at low densities. This is, however, not unexpected since the low-density regime is completely dominated by the charged impurity induced random puddles of compressible and incompressible regions.

We contend that this failure of the standard many-body theoretical techniques is due to the fact that they do not incorporate the effects of the inhomogeneous charge distribution which has been shown to exist in bilayer graphene [5–7]. To demonstrate how vital this effect is, and to characterize the disorder-induced carrier density inhomogeneities and the nonlinear screening of the disorder potential we have developed a self-consistent TFT for $\frac{d\mu}{dn}$ based on the full four band model of BLG that is a generalization of the theory presented in Ref. 7. The use of the full four band model, rather than the simplified two band model [8], is essential to accurately represent the non-quadratic nature of the low-energy band structure in the presence of a band gap, and to calculate the compressibility in the presence of strong disorder since there will be regions where the local carrier density is above the applicable range of the two band model. In this approach, the carrier density landscape is obtained by minimizing a Thomas-Fermi energy functional of the density $n(\mathbf{r})$ that includes a term due to the presence of disorder. The TFT is similar in spirit to the DFT [16–18], but in TFT the kinetic energy operator is also replaced by a functional $E_K[n]$. This simplification makes the TFT valid only when the density profile varies on length scales larger than the Fermi wavelength, i.e. when $|\nabla n/n| < k_F$, where $k_F = \sqrt{\pi n}$ is the Fermi wave vector. This condition is satisfied for gapped BLG. On the other hand, the TFT is computationally much more efficient than DFT and as a consequence is the only method that allows the calculation of disorder-averaged quantities taking into account the nonlinear screening effects. A full DFT theory for this disordered problem is computationally intractable, and in any case, unnecessary because the

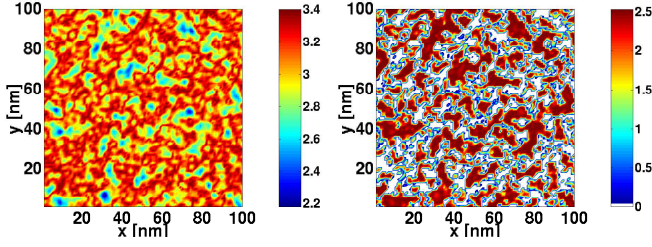


FIG. 2. (Color online.) Local $\frac{d\mu}{dn}$ for a single disorder realization at the charge-neutrality point ($\langle n \rangle = 0$). The units are eV/nm². The incompressible (and insulating) regions where $n = 0$ are shown in white. The left-hand plot has $u = 0$, the right-hand plot has $u = 40$ meV, and $n_i = 3 \times 10^{11}$ cm⁻² for both.

TFT is valid for the system.

The TFT energy functional is given by

$$E[n] = E_K[n(\mathbf{r})] + \frac{e^2}{2\kappa} \int d\mathbf{r}' \int d\mathbf{r} \frac{n(\mathbf{r})n(\mathbf{r}')}{|\mathbf{r} - \mathbf{r}'|} + \frac{e^2}{\kappa} \int d\mathbf{r} V_D(\mathbf{r})n(\mathbf{r}) - \mu \int d\mathbf{r} n(\mathbf{r}). \quad (3)$$

where $e^2 V_D/\kappa$ is the bare disorder potential which is assumed to be due to the Coulomb interaction with randomly distributed charged impurities with no spatial correlation and an equal probability of being positively or negatively charged. The first term is the kinetic energy where $\epsilon_K[n(\mathbf{r})] = \delta E_K[n(\mathbf{r})]/\delta n$ is the single-particle dispersion as a function of the density, the second term is the Hartree part of the electron-electron Coulomb interaction, the third is the contribution due to the disorder potential, and μ is the chemical potential. We neglect exchange and correlation terms [19] since, as we shall show below, $\frac{d\mu}{dn}$ is predominantly determined by the proportion of the sample which is incompressible and the inclusion of the exchange and correlation terms will not change this. The ground state density landscape is identified by the equation $\delta E/\delta n = 0$. Taking the variational derivative of $E[n]$ we find:

$$\frac{\delta E}{\delta n} = \epsilon_K[n(\mathbf{r})] + \frac{e^2}{2\epsilon} \int \frac{n(\mathbf{r}')d\mathbf{r}'}{|\mathbf{r} - \mathbf{r}'|} + \frac{e^2}{\epsilon} V_D(\mathbf{r}) - \mu. \quad (4)$$

Within our formalism it is fairly easy to assume the presence of spatial correlations among the impurities, and the presence of correlations has important effects on the transport properties of BLG [20–22], however they do not modify the qualitative effects that the disorder has on the compressibility.

Assuming that the clean $\frac{d\mu}{dn}$ is valid locally, in Fig. 2 we show the spatial profile of $\frac{d\mu}{dn}$ for a single realization of disorder ($n_i = 3 \times 10^{11}$ cm⁻²) for the gapless regime (left plot) and the gapped case with $u = 40$ meV (right plot). The white regions are incompressible and correspond exactly to the insulating portion of the graphene,

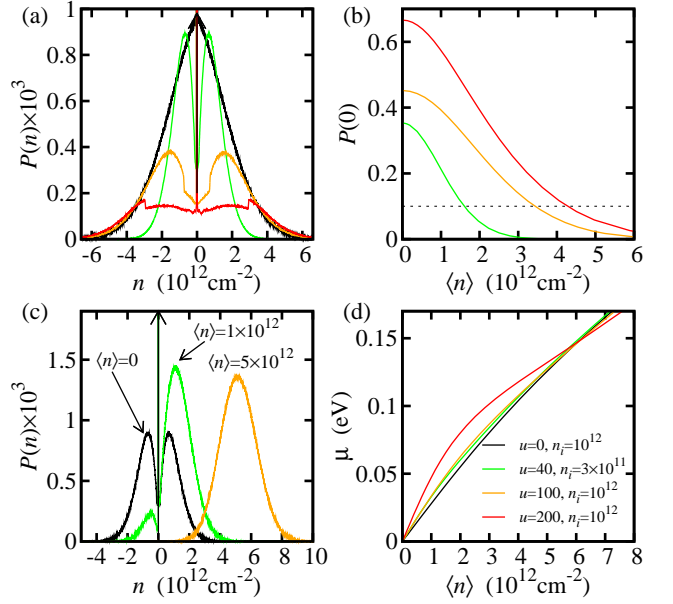


FIG. 3. (Color online). (a) $P(n)$ at the charge neutrality point $\langle n \rangle = 0$ for different values of u and n_i . The arrow at $n = 0$ represents the very narrow peak at $n = 0$ and $u \neq 0$ whose height is orders of magnitude larger than the y -scale used. (b) $P(n = 0)$ for parameters corresponding to Fig. 1(b–d). A dotted line at $P(0) = 0.1$ is provided as a guide to the eye. (c) Evolution of $P(n)$ with doping $\langle n \rangle$ for $u = 40$ meV and $n_i = 5 \times 10^{11}$ cm⁻². (d) μ as a function of doping. The legend in (d) applies also to panels (a) and (c).

i.e. the region where $n = 0$. It is immediately noticeable that in the presence of a band gap, there are large incompressible regions and that these are not present in the gapless case.

By considering several disorder realizations we can calculate disorder averaged quantities and, in particular, the probability distribution function of the local carrier density $P(n)$. This function can be used to compute the average density (doping) as $\langle n \rangle = \int n' P(n') dn'$. As shown in Fig. 3(a), $P(n)$ is trimodal for $\langle n \rangle = 0$ in the gapped regime: it exhibits a large peak shown by an arrow at $n = 0$ that quantifies the fraction of the sample occupied by insulating regions (i.e. regions with no carriers) and two much smaller and broader peaks centered around values of n that are determined by the nonlinear screening of the disorder potential which therefore depend both on u and n_i . Fig. 3(a) also shows that $P(n)$ has a jump for $n = \tilde{n}$. As the doping increases the fraction of the sample area covered by insulating regions $P(n = 0)$ decreases as shown in Fig. 3(b). Notice the factor of 10^3 difference in the vertical scale between Fig. 3(a) and Fig. 3(b). Figure 3(c) shows the evolution of $P(n)$ with $\langle n \rangle$. For finite doping, the distribution becomes asymmetric in n and becomes unimodal only at relatively large doping. In the unimodal regime, $P(n)$ is well approximated by a Gaussian centered around $\langle n \rangle$.

Experimental probes such as capacitance measurement and scanning SET microscopy simultaneously probe an area of the sample which is significantly larger than the puddle size as predicted in the TFT and measured by STM [6]. Therefore an averaging procedure must be implemented to replicate $\frac{d\mu}{dn}$ as a function of $\langle n \rangle$ as measured in these experiments. By disorder averaging the TFT results, we obtain the dependence of the average chemical potential $\langle \mu \rangle$ (which is identical to the μ in Eq. (3)) with respect to the average density $\langle n \rangle$. Because of the nonlinear screening the relation between the average chemical potential $\langle \mu \rangle$ and $\langle n \rangle$ is also modified by the value of the gap and the strength of disorder, as shown in Fig. 3(d). Thus, the TFT results clearly show the inhomogeneous nature of the carrier density landscape in BLG in the presence of disorder. Using the TFT we therefore calculate the average $\left\langle \frac{d\mu}{dn} \right\rangle = \frac{d\langle \mu \rangle}{d\langle n \rangle}$, that closely simulates the way in which $\langle d\mu/dn \rangle$ is obtained in both capacitance measurements [4] and in SET spectroscopy [5]. We emphasize that this particular averaging procedure, simulating the experimental conditions, is simply inaccessible to any type of theories invoking a homogeneous charge landscape to obtain a many-body self-energy or broadening unless the density fluctuations become very small.

Figures 1(a)–(d) show the calculated $\frac{d\mu}{dn}$ using TFT as a dashed-dotted line. We see immediately that it exhibits qualitatively different behavior from the BA and SCBA, and at low density it shows a broad peak in qualitative agreement with the experimental data. Comparison of Figs. 1(b)–(d) with Fig. 3(b) shows that the deviation of the diagrammatic theories from the TFT occurs when $P(0) > 0.1$, indicating that the presence of insulating, incompressible regions is the dominating feature for the compressibility at low density. In Fig. 1(e), we show our TFT calculated density fluctuation characterized by the root-mean-square value n_{rms} as a function of the average density (i.e. doping). This clearly establishes that, when a band gap is present and as the fluctuation (i.e. inhomogeneity) becomes large with decreasing average density, the calculated TFT results for $\frac{d\mu}{dn}$ start deviating substantially from the many-body perturbative ensemble averaged results, and when $n_{\text{rms}}/n \approx 0.5$ one must carry out the nonlinear screening theory to obtain the compressibility.

Therefore, we identify two different reasons for the failure of the standard diagrammatic methods in gapped BLG systems. The first is the presence of strong density inhomogeneity characterized by the parameter n_{rms}/n . When $n_{\text{rms}}/n > a$ with $a \sim 1$, the ground state cannot be assumed to be homogeneous and therefore the diagrammatic approaches fail to quantitatively describe the experimental situation [1]. The exact value of a depends on the experimental quantity under consideration and the details of the experimental conditions. The sec-

ond reason for failure is the existence of a random mixed inhomogeneous state where insulating (incompressible) and metallic (compressible) regions coexist in the presence of a band gap of the order of or smaller than the disorder strength. The diagrammatic methods fail qualitatively since they cannot take this into account. For the compressibility, comparison of Fig. 3(b) with Figs. 1(b–d) shows that the critical fraction of the sample area covered by insulating regions for the diagrammatic methods to give results in strong qualitative disagreement with experiments is $P(0) > 0.1$. Thus, disorder has a much stronger qualitative effect at low carrier densities on the compressibility of BLG [4, 5] than the monolayer [10] since BLG, by virtue of being a gapped system, can be in the random mixed state of gapped and ungapped spatial regions at low densities.

In conclusion, we have demonstrated that the nonlinear nature of the screening of an external disorder potential in gapped bilayer graphene and the resulting charge inhomogeneity are crucial in understanding the ground state electronic properties for a wide range of experimentally relevant carrier density. In particular, standard many-body diagrammatic techniques assume that the density profile is homogeneous in both the screening and the Green's function, and therefore give qualitatively incorrect predictions for the compressibility in the presence of an external band gap. In contrast, the TFT retains the inhomogeneity and non-linear screening of the density distribution in the energy functional $E[n(\mathbf{r})]$ and therefore captures the essential physics of the system. Finally, we point out that although we have presented results where the disorder potential is induced by random charged impurities, our general conclusion will remain valid for any form of disorder which produces a scalar potential perturbation to the clean Hamiltonian, such as corrugations in the graphene sheet [23].

We thank the US-ONR and NRI-SWAN for financial support. E.R. acknowledges support from the Jeffress memorial Trust, Grant No. J-1033. E.R. and D.S.L.A acknowledge the hospitality of the KITP, supported in part by the National Science Foundation under Grant No. PHY11-25915, where part of the work was carried out. Computations were conducted in part on the SciClone Cluster at the College of William and Mary.

-
- [1] S. Das Sarma, S. Adam, E. H. Hwang, and E. Rossi, *Rev. Mod. Phys.* **83**, 407 (2011).
 - [2] D. S. L. Abergel, V. Apalkov, J. Berashevich, K. Ziegler, and T. Chakraborty, *Adv. Phys.* **59**, 261 (2010).
 - [3] D. S. L. Abergel, *ArXiv e-prints* (2012), arXiv:1202.5313 [cond-mat.mes-hall].
 - [4] E. A. Henriksen and J. P. Eisenstein, *Phys. Rev. B* **82**, 041412 (2010).
 - [5] J. Martin, B. E. Feldman, R. T. Weitz, M. T. Allen, and

- A. Yacoby, Phys. Rev. Lett. **105**, 256806 (2010).
- [6] A. Deshpande, W. Bao, Z. Zhao, C. N. Lau, and B. J. LeRoy, Appl. Phys. Lett. **95**, 243502 (2009).
 - [7] E. Rossi and S. Das Sarma, Phys. Rev. Lett. **107**, 155502 (2011).
 - [8] E. McCann and V. I. Fal'ko, Phys. Rev. Lett. **96**, 086805 (2006).
 - [9] A. L. Efros, Solid State Commun. **67**, 1019 (1988).
 - [10] J. Martin, N. Akerman, G. Ulbricht, T. Lohmann, J. H. Smet, K. von Klitzing, and A. Yacoby, Nat. Phys. **4**, 144 (2008).
 - [11] E. Rossi and S. Das Sarma, Phys. Rev. Lett. **101**, 166803 (2008).
 - [12] R. Asgari, M. M. Vazifeh, M. R. Ramezanali, E. Davoudi, and B. Tanatar, Phys. Rev. B **77**, 125432 (2008).
 - [13] E. H. Hwang, B. Y.-K. Hu, and S. Das Sarma, Phys. Rev. Lett. **99**, 226801 (2007).
 - [14] D. S. L. Abergel, H. Min, E. H. Hwang, and S. Das Sarma, Phys. Rev. B **85**, 045411 (2012).
 - [15] The data in Ref. 4 is a capacitance measurement and in order to extract $\frac{d\mu}{dn}$ we need accurate knowledge of experimental parameters such as the impurity density, band gap, stray capacitance, and dielectric environment which are known only approximately in experiments. Therefore the experimental data shown here does not correspond exactly to the parameters used in the calculations and we cannot expect quantitative agreement.
 - [16] P. Hohenberg and W. Kohn, Phys. Rev. **136**, B864 (1964).
 - [17] W. Kohn and L. J. Sham, Phys. Rev. **140**, A1133 (1965).
 - [18] W. Kohn, Rev. Mod. Phys. **71**, 1253 (1999).
 - [19] G. Borghi, M. Polini, R. Asgari, and A. H. MacDonald, Phys. Rev. B **82**, 155403 (2010).
 - [20] Q. Li, E. H. Hwang, E. Rossi, and S. Das Sarma, Phys. Rev. Lett. **107**, 156601 (2011).
 - [21] J. Yan and M. S. Fuhrer, Phys. Rev. Lett. **107**, 206601 (2011).
 - [22] Q. Li, E. H. Hwang, and E. Rossi, ArXiv e-prints (2012), arXiv:1202.5546 [cond-mat.mes-hall].
 - [23] M. Gibertini, A. Tomadin, F. Guinea, M. I. Katsnelson, and M. Polini, ArXiv e-prints (2011), arXiv:1111.6280 [cond-mat.mes-hall].